

## Coastal flooding in Scituate (MA): A FVCOM study of the 27 December 2010 nor'easter

Robert C. Beardsley,<sup>1</sup> Changsheng Chen,<sup>2,3</sup> and Qichun Xu<sup>2</sup>

Received 17 February 2013; revised 30 September 2013; accepted 15 October 2013; published 13 November 2013.

[1] A nested Finite-Volume Coastal Ocean Model (FVCOM) inundation forecast model has been developed for Scituate (MA) as part of the Northeast Coastal Ocean Forecast System (NECOFS). Scituate Harbor is a small coastal lagoon oriented north-south with a narrow entrance (with opposing breakwaters) opening eastward onto Massachusetts Bay and the Gulf of Maine. On 27 December 2010, a classic nor'easter produced a  $\sim 0.9$  m high surge, which when added to the  $\sim 1.5$  m high tide and seasonal higher mean water level, produced significant inundation in Scituate. The Scituate FVCOM inundation model includes flooding/drying, seawall/breakwater, and wave-current interaction capabilities, and was driven by one-way nesting with NECOFS. Hindcasts of the 27 December nor'easter event were made with two different resolution Scituate FVCOM grids with and without inclusion of wave-current interaction to examine the influence of spatial resolution and model dynamics on the predicted flooding. In all simulations, a wind-driven coastal current flowed southward across the harbor entrance, with an attached separation eddy forming downstream of the northern breakwater and rapid decrease in wave energy entering the harbor. With wave-current interaction, the southward coastal current was strongly enhanced and currents within the separation eddy increased to more than 1 m/s, making it highly nonlinear with large lateral shears. Comparisons of the model water elevation time series with harbor tide station measurements showed that inclusion of wave-current interaction increased the peak model surge by  $\sim 8$  cm, in closer agreement with the observed peak.

**Citation:** Beardsley, R. C., C. Chen, and Q. Xu (2013), Coastal flooding in Scituate (MA): A FVCOM study of the 27 December 2010 nor'easter, *J. Geophys. Res. Oceans*, 118, 6030–6045, doi:10.1002/2013JC008862.

### 1. Introduction

[2] Coastal inundation in New England is generally caused by some combination of high tides, large wind waves and swell, storm surge, heavy rains, and high river discharge. While tropical storms occasionally passing northward along the New England coast can cause inundation, strong extratropical cyclones (e.g., nor'easters) cause significant coastal inundation each year, with major damage to property and infrastructure, and some loss of life. These low-pressure storms typically form between October and April as cold dry continental air meets warmer moist

marine air along the U.S. southeast coast, then deepen and grow in size as they move up along the northeast coast. The stronger storms can exhibit explosive cyclogenesis (with pressure drops of  $\sim 18$  hPa or greater in 24 h), some features of tropical storms (e.g., a circular core and small eye), and strong northeasterly winds (with hurricane-strength gusts) over the ocean ahead of the storm.

[3] The National Weather Service regional Weather Forecast Offices (WFOs) in Taunton (MA) and Grey (ME) have primary responsibility for issuing marine weather forecasts and warnings in New England. In 2008, these two WFOs initiated a program to help improve their capability to forecast coastal inundation. They selected Scituate (MA) as the first of two coastal towns to be pilot sites for establishing an “end-to-end” coastal inundation prediction model system that could be later expanded to other sites in New England. As part of this effort, the Taunton WFO in December 2008 installed a tide gauge station in Scituate Harbor, a weather station near the harbor entrance, and water level staffs in the flood zone around the harbor, to obtain water level and wind data during inundation events.

[4] The Northeast Regional Association of Coastal Ocean Observing Systems (NERACOOS) was established in 2008 as part of the National Oceanic and Atmospheric Administration (NOAA) Integrated Ocean Observing System (IOOS). As part of NERACOOS, a team of

Additional supporting information may be found in the online version of this article.

<sup>1</sup>Department of Physical Oceanography, Woods Hole Oceanographic Institution, Woods Hole, Massachusetts, USA.

<sup>2</sup>School for Marine Science and Technology, University of Massachusetts-Dartmouth, New Bedford, Massachusetts, USA.

<sup>3</sup>International Center for Marine Studies, Shanghai Ocean University, Shanghai, China.

Corresponding author: R. C. Beardsley, Department of Physical Oceanography, Woods Hole Oceanographic Institution, Woods Hole, MA 02543, USA. (rbeardsley@whoi.edu)

©2013. American Geophysical Union. All Rights Reserved.  
2169-9275/13/10.1002/2013JC008862

investigators at the University of Massachusetts-Dartmouth (UMassD) and the Woods Hole Oceanographic Institution (WHOI) developed the Northeast Coastal Ocean Forecast System (NECOFS) to produce 3 day forecasts of the surface forcing, surface water elevation, and 3-D currents and water properties. Built around the unstructured-grid Finite-Volume Coastal Ocean Model (FVCOM, *Chen et al.* [2003]), NECOFS started making experimental forecasts in late 2008 and now includes an unstructured-grid surface wave module, multigrid nesting, data assimilation methods, a third-generation regional grid, and advanced coding for improved computational efficiency.

[5] In collaboration with the Taunton WFO, we built a high-resolution coastal inundation forecast model system for Scituate (called Scituate FVCOM) that would be driven by one-way nesting with the regional NECOFS. Scituate FVCOM includes flooding/drying and coupled wave-current interaction. Hindcast studies of coastal flooding in Scituate caused by nor'easters on 25 May 2005 and 18 April 2007 (the "Patriots' Day Storm") have been conducted using FVCOM, ADCIRC (ADvanced CIRCulation model), and SELFE (Semi-implicit Eulerian-Lagrangian Finite Element model) (see *Chen et al.* [2013], this issue) as part of the IOOS-funded super-regional Coastal Modeling Testbed (<http://testbed.sura.org/>). We describe here the Scituate FVCOM inundation forecast system in more detail and its hindcast of coastal inundation caused by the 27 December 2010 extratropical storm.

[6] This paper is organized as follows. Descriptions of NECOFS, its structure, FVCOM-SWAVE, and the Scituate inundation model are presented in section 2, followed by a short description of the 27 December 2010 storm in section 3. The hindcast results, including waves, water elevation, currents, and transport without and with wave-current interaction, are presented in section 4. A discussion of the results is given in section 5, followed by conclusions in section 6.

## 2. NECOFS Inundation Model System

### 2.1. NECOFS

[7] NECOFS is an integrated atmosphere/surface wave/ocean model system designed for the northeast U.S. coastal region, covering a computational domain from central New Jersey to the eastern end of the Nova Scotian Shelf. The core of this system is the Finite-Volume Coastal Ocean Model (FVCOM) developed by *Chen et al.* [2006a, 2006b]. FVCOM features an unstructured triangular grid in the horizontal and a generalized terrain-following coordinate in the vertical, and solves the integral form of the governing equations by second-order accurate flux-based finite-volume methods [*Kobayashi et al.*, 1999; *Hubbard*, 1999]. Time integration is done using the modified explicit fourth-order Runge-Kutta time stepping scheme. Vertical mixing is simulated using the modified *Mellor and Yamada* [1982] level 2.5 (MY-2.5) and horizontal mixing is calculated using the *Smagorinsky* [1963] turbulent closure scheme. In this study, FVCOM (version 3.1) is integrated using a mode-split solver in which external and internal modes are advanced in tandem at different time steps (with a ratio of external to internal time steps of 5).

[8] The NECOFS domain spans the Scotian Shelf/Gulf of Maine/Georges Bank/New England Shelf region

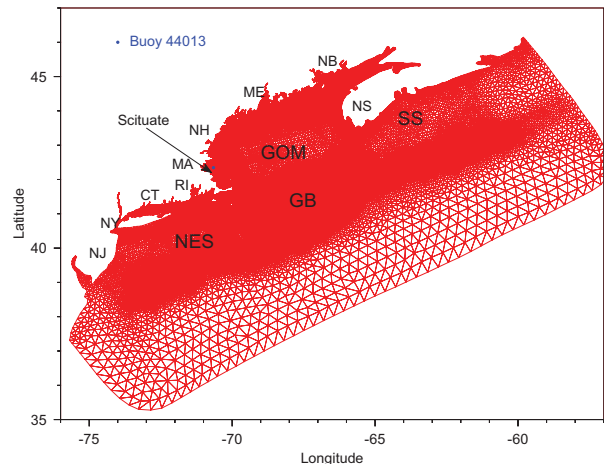


**Figure 1.** Map showing the NECOFS regional FVCOM (GOM3) grid, Scituate, U.S. states, and Canadian provinces. Model domain includes the Scotian Shelf (SS), Gulf of Maine (GOM), Georges Bank (GB) and the New England Shelf (NES). GOM3 has 4860 nodes and 91258 cells. The blue dot shows the location of NDBC buoy 44013.

(Figure 1). The GOM3 horizontal grid used in this study has a resolution (measured by the length of the longest edge of a triangular cell) that varies from 0.3 to 1.0 km in the coastal region up to a maximum of 10 km near the outer boundary. The vertical grid features a total of 45 layers [*Chen et al.*, 2011]. In regions with depth greater than 225 m, 10 uniform layers (5 m thick) are used near the surface and five uniform layers (5 m thick) near the bottom, respectively, to better resolve these layers. In regions of depth less than 225 m, a sigma distribution with a uniform layer thickness is used. The coordinate transition thus occurs smoothly at a depth of 225 m where all layers have a uniform thickness of 5 m. The mean water depth at each node was determined using the U.S. Geological Survey (USGS) 15-arcsec digital bathymetry data set [*Roworth and Signell*, 1998], with a minimum depth of 3 m applied at the coast. A maximum depth cutoff of 1500 m is imposed in the slope region south of the shelf break.

[9] NECOFS is forced by tides at the open boundary, wind stress, heat flux, net precipitation minus evaporation flux and atmospheric pressure at the surface, local river runoff along the coast, and upstream inflow on the Scotian Shelf. The tidal forcing includes the dominant semidiurnal (M2, N2, S2, K2) and diurnal (K1, O1, P1, Q1) tidal constituents determined at the boundary nodes through interpolation of the *Egbert and Erofeeva* [2002]  $1/6^\circ$  inverse tidal model results (see *Chen et al.* [2011] for a detailed description of the regional tidal dynamics).

[10] Surface forcing fields were computed on a  $9 \text{ km} \times 9 \text{ km}$  grid using the National Centers for Environmental Prediction (NCEP)/National Center for Atmospheric Research (NCAR) Weather Research and Forecast (WRF) mesoscale model and the Medium Range Forecast planetary boundary layer scheme [*Hong and Pan*, 1996] with assimilation of weather buoy data. These fields were then interpolated to the FVCOM grid [*Chen et al.*, 2005]. The wind stress, sensible, and latent heat fluxes were computed using the COARE2.6 bulk flux parameterizations [*Fairall et al.*,

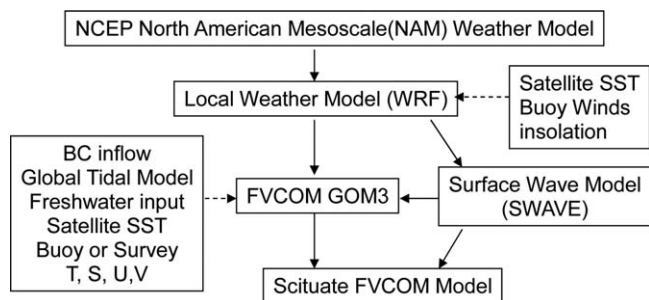


**Figure 2.** Schematic of NECOFS for Scituate inundation simulation. Dashed arrows indicate flow of data used for assimilation and/or boundary conditions.

1996]. The surface shortwave radiation heat flux was output from WRF with subsequent calibration for the daily mean using the International Satellite Climatology Cloud Project (ISCCP) product [Hu, 2009]. WRF was run with inclusion of the NOAA High-resolution Blended Analysis of Daily sea surface temperature (SST) product so that the WRF longwave radiation flux was used directly without calibration. Surface precipitation was obtained from WRF. WRF was run with a time step of 1 min.

[11] Forty-nine major rivers contribute to the fresh water input along the coast in the regional FVCOM GOM3. The river geometry is resolved upstream to where the salinity is zero and the discharge is specified using the USGS data every 15 min. The transport across the upstream Scotian Shelf boundary is a combination of alongshore flow in geostrophic balance with the cross-shelf hydrography [Smith and Schwing, 1991; Loder et al., 2003] and wind-driven flow [Schwing, 1989; Pringle, 2006]. This upstream boundary condition was updated every 30 s.

[12] Bottom stress is computed using the quadratic drag law with the horizontal velocities in the lowest layer and the drag coefficient determined using the logarithmic law of the wall formulation with a spatially varying bottom roughness length  $z_o$ . The value of  $z_o$  is computed as a function of bottom depth. In regions less than 40 m deep,  $z_o$  was set to 0.3 cm. In bottom depths between 40 and 100 m,  $z_o$  decreased monotonically and was set to 0.001 cm at depths greater than 100 m. The resulting  $z_o$  at 60 m bottom depth is  $\sim 0.06$  cm, consistent with the bottom boundary layer measurements made on Georges Bank [Werner et al., 2003; Chen et al., 2001, 2011].

[13] FVCOM originally included the flooding/drying process for tidally driven estuarine applications [Chen et al., 2003]. For more complex coastal ocean and inundation applications (e.g., Scituate), an unstructured-grid finite-volume surface wave model (SWAVE) based on SWAN (Simulating Waves Nearshore model) [Qi et al., 2009] and a module to simulate flow around and over breakwaters and groynes [Ge et al., 2012] have been developed. The regional SWAVE is run on the same grid as NECOFS with boundary forcing from Wave Watch III (WWIII) with the following configuration: 3.0 s time step; 36 direction bins; 20 discrete frequencies ranging from 0.05 to 0.5 cps; and the JONSWAP friction formulation with coefficient of 0.067 [Qi et al., 2009]. WWIII is configured for the larger North Atlantic domain [Sun et al., 2013] and driven by a blend of regional WRF and larger-scale

NCEP forcing. The regional SWAVE is run through decoupling with regional FVCOM to provide the wave boundary forcing for Scituate FVCOM (see below). The NECOFS setup for the Scituate inundation forecast system is shown in Figure 2 (See [http://fvcom.smast.umassd.edu/research\\_projects/NECOFS/index.html/](http://fvcom.smast.umassd.edu/research_projects/NECOFS/index.html/) for more information about NECOFS.).

## 2.2. Scituate FVCOM

[14] Scituate Harbor is located  $\sim 20$  km southeast of Boston Harbor along the south shore of Massachusetts Bay. The harbor is shallow (average depth  $\sim 3$  m) and aligned  $\sim$ north-south, with a northern basin (max. depth  $\sim 4.5$  m) and smaller southern basin (max. depth  $\sim 5.5$  m) (Figure 3). The Edward Foster Road causeway (transect c1–c2) separates the harbor from a large marsh (called the Kent Street Marshes). The southern harbor is connected to the marsh by a shallow, narrow channel (width  $\sim 10$  m, maximum depth  $\sim 1.7$  m). The water depth is referenced to NAVD88, which was estimated by the average value of NAVD88 at Boston and Plymouth (MA).

[15] Scituate Harbor is formed by two promontories, Cedar Point to the north and a pair of headlands (First Cliff and Second Cliff) along the south. Seawalls have been built along much of the coastal side of these promontories. The harbor is entered through a set of three breakwaters (two on

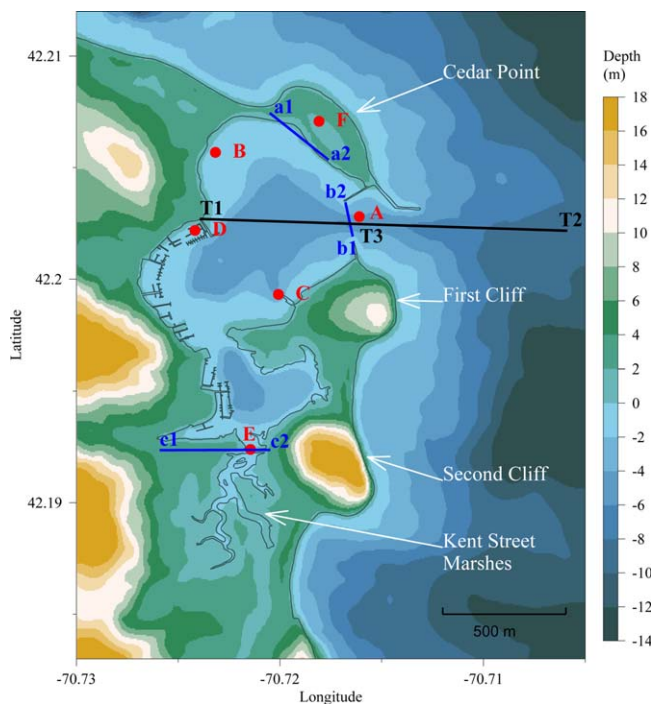


**Figure 3.** Bathymetric map of Scituate Harbor and elevation of surrounding land. Red lettered dots denote locations of stations where model results are shown, the blue letters (a1–a2; b1–b2, and c1–c2) denote transport sections through which volume flux were computed. Station C is located at the tide station on the Stellwagen Bank National Marine Sanctuary dock (Table 1). The black line labeled T1–T2 denotes the cross-harbor transect along which model results are plotted. T3 is located between the entrance breakwaters.

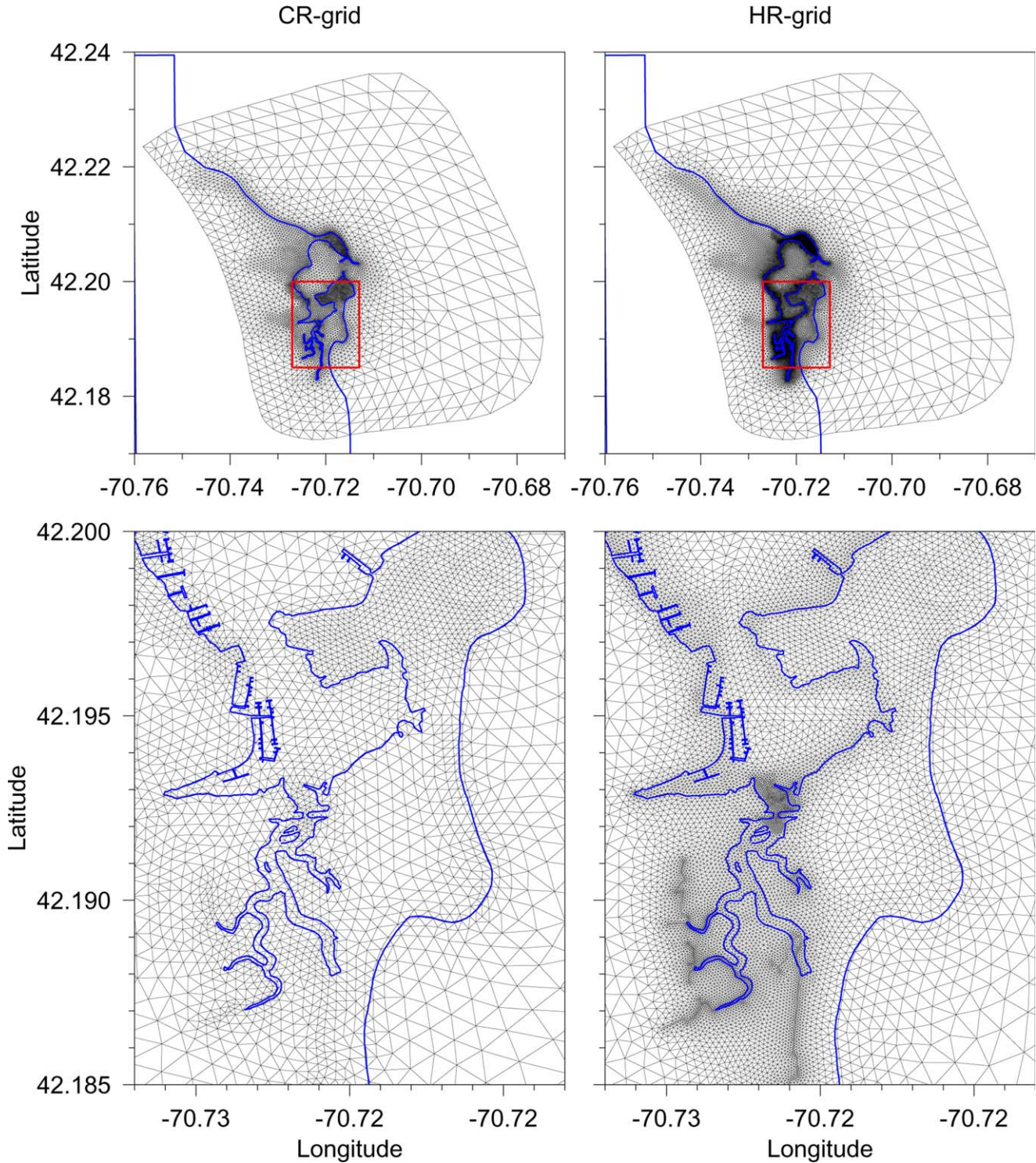


**Figure 4.** Scituate Harbor coarse-resolution (CR) and high-resolution (HR) grids. The coastline is indicated by the blue curve.

the northern side and one on the southern side, Figure 3), with a 60 m wide navigation channel running clockwise around the edge of the First Cliff tidal mudflats into the southern basin, with depth ranging from about 2 to 3.5 m. The entrance breakwaters significantly reduce the penetration of large waves and alongshore currents generated during strong storms. The harbor is used by recreational and

commercial boaters and researchers at the Stellwagen National Marine Sanctuary.

[16] We constructed two Scituate FVCOM inundation grids for this hindcast study to test the sensitivity of the modeled inundation to grid resolution. The coarse-resolution (CR) grid (Figure 4) has a horizontal resolution of 10 m to 1 km, a total of 5620 nodes, a maximum depth of ~22 m

**Table 1.** Number of Nodes, Triangular Cells, and the Areas of the Smallest and Largest Cells in the Scituate Inundation Coarse-Resolution (CR) and High-Resolution (HR) Grids<sup>a</sup>

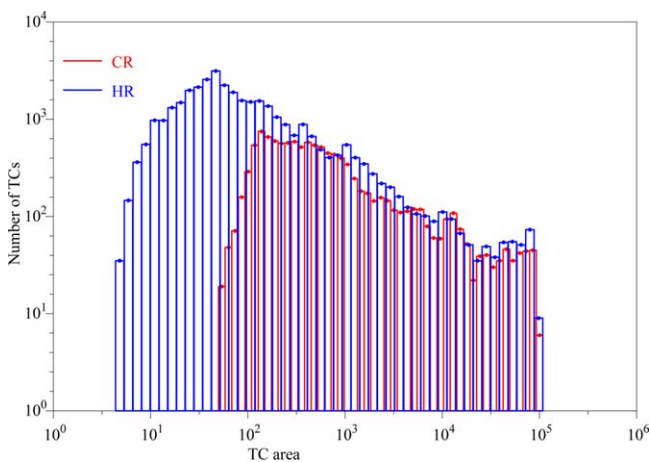
Grid	Nodes	Number TCs	TC Min Area (m <sup>2</sup> )	TC Max Area (m <sup>2</sup> )
CR	5620	11,153	49.78	108,038.25
HR	17,286	34,487	4.32	108,038.25

<sup>a</sup>There are about two triangular cells for each node.

along the open inner-shelf boundary, and a maximum elevation of  $\sim 23$  m on the land boundary. The high-resolution (HR) grid has finer horizontal resolution primarily within the harbor and coastal area, with the minimum grid size reduced to 2 m with little or no change toward the outer land boundary and the inner-shelf boundary with GOM3 (Table 1 and Figure 5). The HR grid has a total of 17,286 nodes and thus required an increase in computational run time of 10 for the December 2010 storm hindcasts (Table 2a). Both CR and HR grids feature a total of 11 sigma layers in the vertical, and the water column is considered “dry” when its thickness becomes less than 5.0 cm.

[17] Both HR and CR Scituate FVCOM grids were constructed using a combination of USGS recent light detection and ranging (LiDAR) bathymetry data (provided by R. Signell, USGS) and land elevation data collected by LiDAR and Google maps. The LiDAR data were collected in 2005–2007 with a horizontal and vertical resolution of 1.0 m and 0.01 cm, respectively. Houses and other features were not included, but the coastal seawalls and three breakwaters in the harbor entrance were included in the grids. The bottom roughness length  $z_o$  was set to 0.3 cm independent of water depth greater than 3 m; in shallower water, the drag coefficient was set to 0.0027.

[18] The Scituate FVCOM inundation grid is driven at the open boundary by one-way nesting with the regional FVCOM GOM3. By making the open boundary cells of the Scituate grid identical to the GOM3 cells, the nesting does not require interpolation and is locally conservative. Scituate surface forcing is obtained through interpolation from the regional WRF forcing fields. The Scituate wave model

**Figure 5.** Histogram of the number of the triangular cells (TCs) as a function of their area (m<sup>2</sup>) in the coarse-resolution (CR) and high-resolution (HR) grids.**Table 2a.** Approximate Computer Run Times for the Different Model Simulations Made in This Study<sup>a</sup>

NECOFS Models	Number of Nodes	Node Chipset	Time (h)
WRF forecast	4	X5670	1.0
WRF hindcast	4	X5670	1.25
GOM3 forecast	4	X5670	1.0
GOM3 hindcast	4	X5670	2.0
WaveWatch III	4	X5670	1.0
GOM3 wave	4	X5670	2.0
Scituate CR forecast	4	E5450	1.25
Scituate HR forecast	8	E5450	4.5
Scituate CR forecast with WCI	4	E5450	16.0
Scituate HR forecast with WCI	8	E5450	102.0

<sup>a</sup>The times listed are for 3 day simulations. The Scituate inundation simulations were made on the UMassD cluster server Dell 5450 and all other simulations made on the cluster server Dell 1950. These servers are described in more detail in Table 2b.

SWAVE uses the same Scituate FVCOM grid and is configured using the regional SWAVE parameters and driven at the outer boundary by significant wave height, peak period, and wave direction output from the regional GOM3 domain SWAVE simulation.

[19] The Scituate FVCOM and SWAVE are dynamically coupled and run in parallel. The coupling is approached by adding the radiation stress in the momentum equations as

$$\frac{du}{dt} - fv = \text{RHS}(u) - \frac{\partial S_{xx}}{\partial x} - \frac{\partial S_{xy}}{\partial y} - \frac{\partial S_{xz}}{\partial z} \quad (1)$$

$$\frac{dv}{dt} + fu = \text{RHS}(v) - \frac{\partial S_{yx}}{\partial x} - \frac{\partial S_{yy}}{\partial y} - \frac{\partial S_{yz}}{\partial z} \quad (2)$$

where  $u$  and  $v$  are the  $x$  and  $y$  components of the water velocity, respectively;  $f$  is the Coriolis parameter; and  $\text{RHS}(u)$  and  $\text{RHS}(v)$  represent all forcing and diffusion terms in the  $u$ - and  $v$ -momentum equations, respectively.  $S_{xx}$ ,  $S_{xy}$ , and  $S_{xz}$  are the  $x$ ,  $y$ , and  $z$  components of the radiation stress in the  $u$ -momentum equation, and  $S_{yx}$ ,  $S_{yy}$ , and  $S_{yz}$  are the  $x$ ,  $y$ , and  $z$  components of the radiation stress in the  $v$ -momentum equation. These radiation stress terms and computational algorithms are described in detail in Warner *et al.* [2008] and Wu *et al.* [2010]. In addition, the surface drag coefficient is calculated by

**Table 2b.** Information About UMassD Cluster Server DELL R410 (Chipset X5670) and Server DELL 1950 (Chipset E5450)

Server	Dell R410	Dell 1950
Chipset	X5670	E5450
CPU family	Nehalem	Harpertown
Processes/node	12	8
CPU/node	2	2
Cores/CPU	6	4
CPU clock (GHz)	2.9	3.0
RAM/node (GB)	12	8
RAM type	DDR3 1333 MHz	DDR2 1333 MHz
Network	Infiniband QDR	Infiniband DDR
Network card	Mellanox ConnectX PCI-E 40 Gbit	Mellanox ConnectX PCI-E 20 Gbit
Theoretical Gflops/node	140	96

**Table 3.** Scituate Harbor Tide Gauge Harmonic Analysis Results<sup>a</sup>

Tide	Period A		Period B	
	Amp (cm)	Phase (o)	Amp (cm)	Phase (o)
O1	11.3 ± 0.4	124.4 ± 2.0	10.6 ± 4.1	121.3 ± 21.0
K1	13.9 ± 0.4	137.4 ± 1.6	18.4 ± 4.4	129.2 ± 15.3
N2	30.0 ± 2.0	307.8 ± 3.9	24.1 ± 3.7	295.9 ± 8.7
H1	18.5 ± 1.9	60.1 ± 6.2		
M2	127.2 ± 2.1	339.8 ± 0.9	132.4 ± 3.4	323.8 ± 1.6
H2	18.1 ± 2.3	247.9 ± 5.8		
S2	19.7 ± 1.9	12.5 ± 5.6	17.0 ± 3.7	356.2 ± 11.9

<sup>a</sup>Harmonic analysis results for Scituate Harbor tide gauge computed for Period A (6 December 2008 to 10 January 2011; 765.2 days) and Period B (11 December 2010 to 10 January 2011; 30.0 days). The predicted tide (including all constituents with  $\text{SNR} \geq 2$ ) accounted for 96–97% of the variance in both periods. The harmonic results shown below for Period B were used to drive the tidal boundary conditions for the CR and HR simulations. The significant higher harmonics all had amplitudes  $\sim 2$  cm or less and were not used. The mean water elevation during Period B was 1.74 m, 10 cm greater than in Period A. The 27 December storm surge contributed  $\sim 1$  m to this higher mean elevation.

$$C_d = [\kappa / \ln(10/z_o)]^2 \quad (3)$$

where the von Karman constant  $\kappa = 0.41$  and  $z_o$  is the sea surface roughness calculated using Donelan's parameterization [Donelan et al., 1993] given as

$$z_o = 3.7 \times 10^{-5} \frac{U_{10}^2}{g} \left( \frac{U_{10}}{C_p} \right)^{0.9} \quad (4)$$

where  $C_p$  is the phase velocity of the peak frequency wave,  $U_{10}$  is the 10 m wind speed and  $U_{10}/C_p$  is defined as the wave age. The bottom stress is calculated using the bottom boundary layer model implemented in Warner et al. [2008]. The time steps to run Scituate FVCOM and SWAVE were 1.0 (external mode) and 3.0 s for the CR cases and 0.2 (external mode) and 0.6 s for the HR cases. The coupling was made on the SWAVE time step. Our inundation forecast was done in two steps: the NECOFS FVCOM GOM3 and SWAVE regional forecast was first made and then its 3 day output was used to drive the Scituate forecast system. The Scituate FVCOM open boundary conditions were updated every internal time step of FVCOM GOM3. Output from NECOFS GOM3 and SWAVE and the Scituate FVCOM and SWAVE simulations were saved every hour. This same approach was used in the hindcast simulations presented in this paper.

[20] Harmonic analysis of the 1.8 year long Scituate Harbor tide gauge data using T\_Tide [Pawlowicz et al., 2002] indicated a significant seasonal increase in the M2 amplitude in winter (Table 3, Period A), with constituents H1 and H2 amplitudes roughly equal to 14% of the M2 amplitude [Foreman et al., 1995; García-Lafuente et al., 2012]. To better simulate the tides during the December 2010 storm period, we forced the tides on the CR and HR grid outer boundary using the amplitude and phase values obtained in an analysis of the 30 day segment of the Scituate Harbor tide gauge data centered on 26 December (Table 3, Period B). All other CR and HR grid outer boundary conditions (surface waves, subtidal currents and elevation,

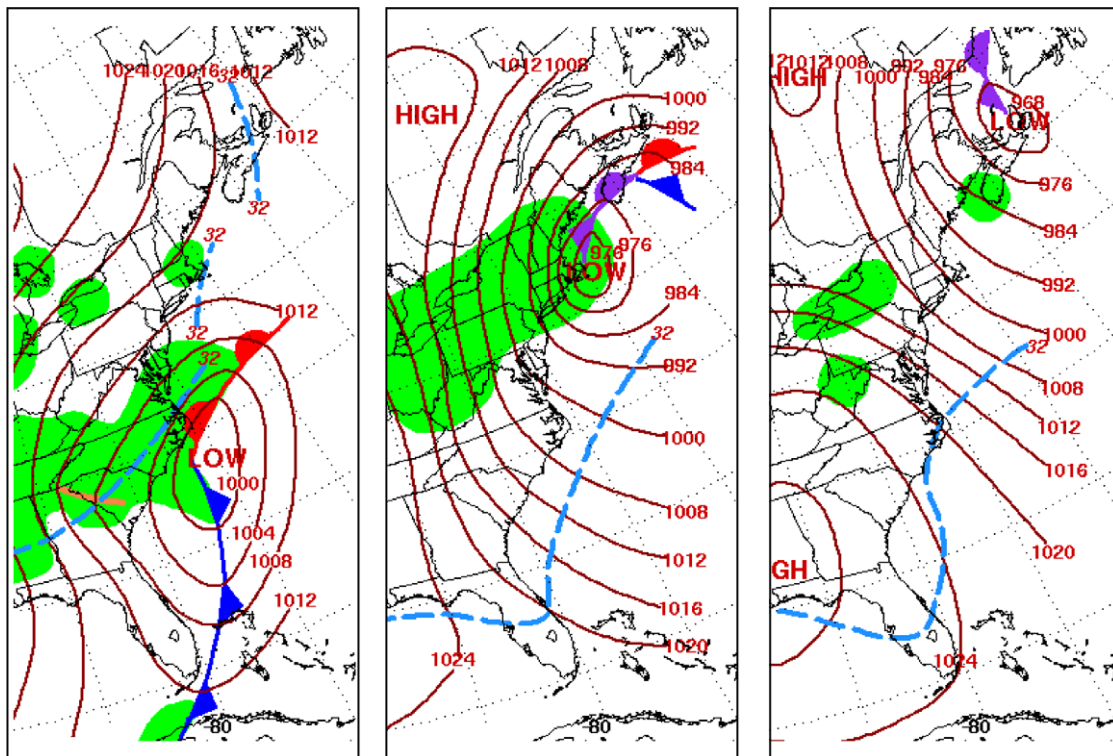


**Figure 6.** Sequence (left to right) of daily weather maps at 7 EST (12 GMT) 26, 27, and 28 December 2010. The blue dashed line indicates the 0°C isotherm and the green shading indicate areas of precipitation within the last 6 h.

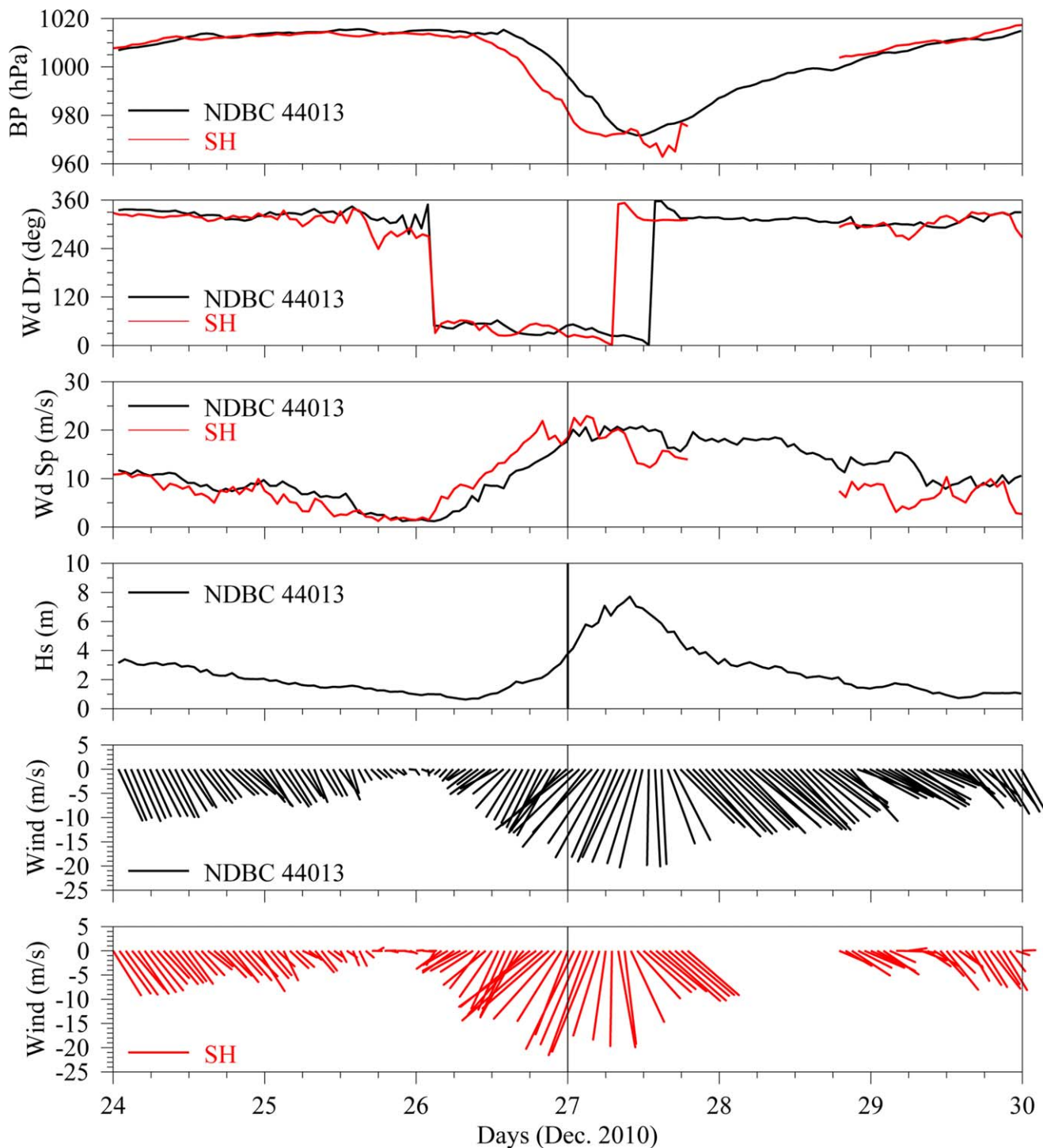


**Figure 7.** Surface wind, barometric pressure, and wave data collected at NDBC 44013 and Scituate Harbor (SH) entrance. From top, barometric pressure (hPa), wind direction (deg), wind speed ( $\text{m s}^{-1}$ ), wave height (m), 44013 vector wind, and SH vector wind. SH time series plotted in red. Time is GMT. Buoy location:  $42.346^\circ \text{ N}$ ,  $70.651^\circ \text{ W}$ .

temperature and salinity) were obtained from the NECOFS FVCOM GOM3 and SWAVE forecasts.

### 3. The 27 December 2010 Storm

[21] This classic nor'easter started as a large extratropical low-pressure system centered off North Carolina on 26

December and strengthens into a gale as it approached Cape Cod and southeastern Massachusetts the next day (Figure 6). The drop in center pressure during this 1 day track over the Mid-Atlantic Bight was roughly  $20 \text{ hPa}$ , almost  $1 \text{ hPa h}^{-1}$ .

[22] Surface weather and wave data collected at the NOAA environmental buoy National Data Buoy Center

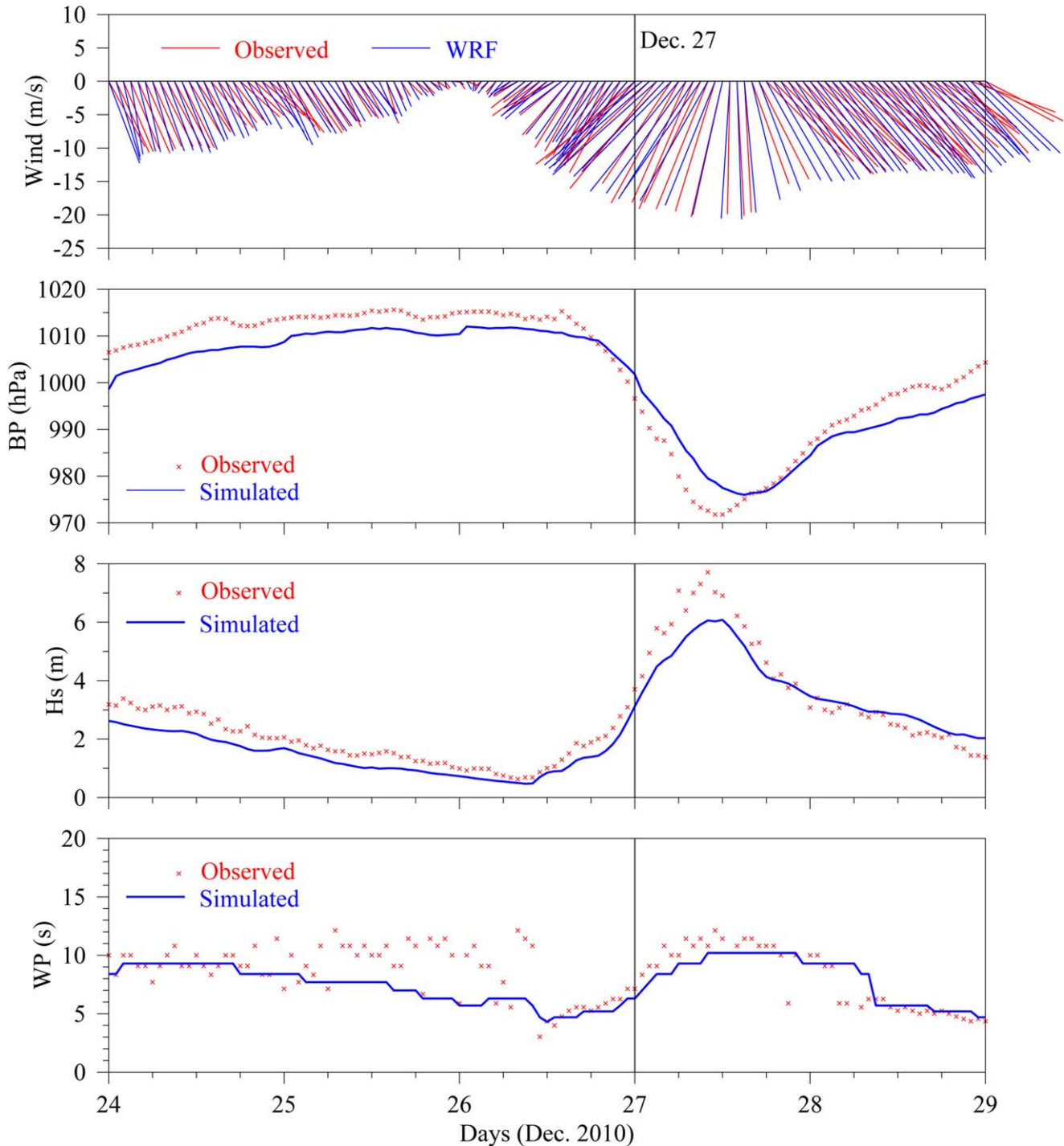


**Figure 8.** Comparison of surface wind, pressure, and wave parameters measured at NDBC 44013 with NECOFS/WRF and SWAVE GOM3 simulations. From the top, wind speed ( $\text{m s}^{-1}$ ), barometric pressure (hPa), significant wave height (m), and peak wave period (s).

(NDBC) 44013 located  $\sim 17$  km NNE of Scituate and at the Scituate Harbor entrance weather station show the passage of this storm (Figure 7). The leading edge of the storm arrived around 02 GMT 26 December, when winds from the northeast started to increase and barometric pressure started to drop at Scituate, with NDBC 44013 lagging by roughly 1 h. Winds at Scituate and 44013 increased to

peaks of  $\sim 22$  and  $\sim 20$  m/s, respectively, the difference due in part to the difference in wind sensor height. Wind gust speeds at both sites increased with wind speed by roughly 20–30% at the higher speeds. Barometric pressure at Scituate dropped from 1013 hPa at 09 GMT 26 December to 971 hPa at 06 GMT the next day, 42 hPa in just 21 h. The pressure drop at 44013 was similar but lagged Scituate by

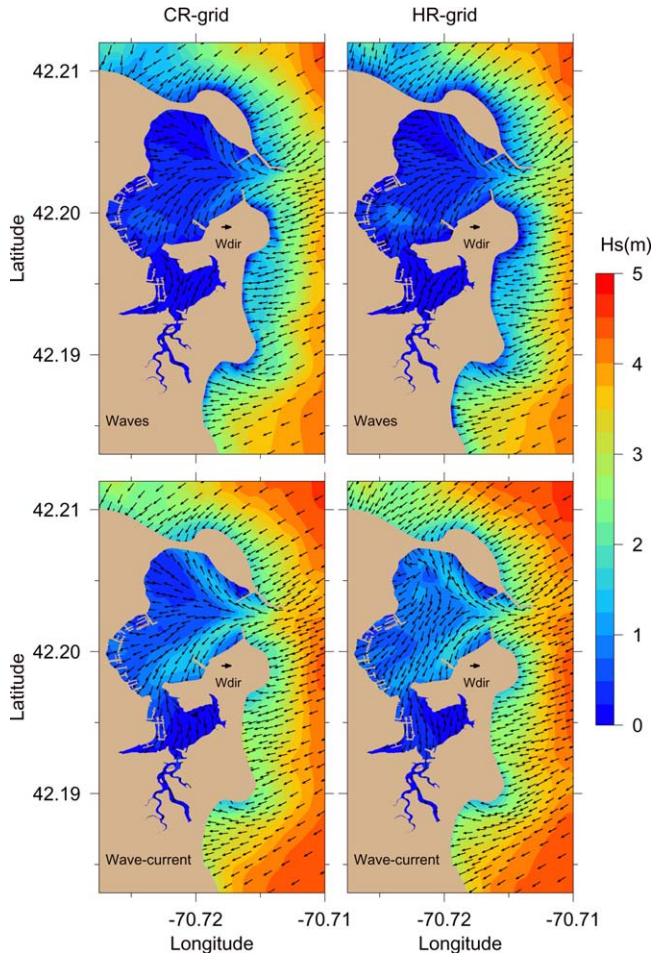


**Figure 9.** Maps of surface wave height (m) and direction (arrows) at 08 GMT 27 December. Left panels: CR-grid; right panels: HR-grid. Top row: wave field without wave-current interaction; bottom row: wave field with wave-current interaction.

roughly 5 h. As the storm center passed Scituate around 8 GMT, the barometric pressure began rising, the winds rapidly shifted to northwest (offshore in Mass Bay) and slowly decreased over the next 24 h. Waves at NDBC 44013 increased to  $\sim 7.5$  m near 10 GMT, then subsided to  $\sim 3.5$  m over the next 24 h due to the northwest winds.

## 4. Model Results

### 4.1. Waves

#### 4.1.1. SWAVE-44013 Comparison

[23] A comparison of the surface weather and wave data measured at NDBC 44013 with the NECOFS and SWAVE hindcast results is shown in Figure 8. At this site, the model captures the observed wind direction well but underestimates the wind speed and pressure drop (by  $\sim 8$  hPa) during the storm arrival and passage 26–27 December. During this same period, the SWAVE-simulated surface wave growth and direction agree with the buoy measurements, but slightly underestimate the peak wave

height and then decay more slowly than observed. The water depth at NDBC 44013 was sufficiently deep ( $\sim 65$  m) that the peak measured and model waves with 10 s periods were deep water waves, which began to sense the bottom near the 40 m isobath. The agreement found at NDBC 44013 during the storm up to early 27 December supports the use of the regional SWAVE hindcast for the Scituate SWAVE boundary forcing (See W. Perrie et al., *Modelling North Atlantic nor'easters with modern wave forecast models, in revision for Journal of Geophysical Research: Oceans*, 2013, for a more complete comparison of SWAVE with 44013 and other buoys in the Gulf of Maine.).

#### 4.1.2. Scituate SWAVE Comparisons

[24] Surface wave hindcasts were made using the two Scituate grids for two cases, waves without wave-current interaction and with wave-current interaction. Maps of the significant wave height distribution and wave direction for the four simulations at the peak of the storm (08 GMT 27 December, at the end of flood tide) are shown in Figure 9. In general, waves reached their maximum heights over the inner shelf and then decreased in amplitude as the waves turned toward the coastline, shoaled, and dissipated, with wave-current interaction allowing large waves to approach

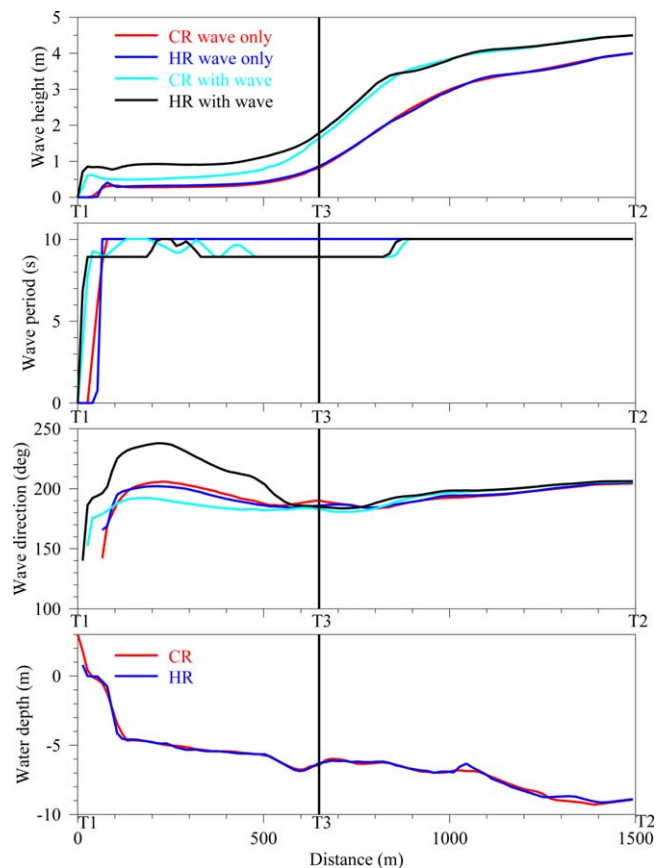


**Figure 10.** Surface significant wave height (m), peak period (s), direction (degrees CCW from E), and bottom depth along transect starting at shore inside the harbor (T1) (0 m) through the entrance breakwaters (T3) (650 m) out to 1500 m (T2) at 08 GMT 27 December for the four cases.

**Table 4.** Model Elevation Comparison Near Scituate Harbor Tide Station<sup>a</sup>

Case	Mean (m)	Std (m)	Max (m)	Min (m)
CRNW	0.313	1.143	2.213	-1.581
HRNW	0.313	1.143	2.213	-1.579
CRWW	0.324	1.130	2.291	-1.538
HRWW	0.297	1.132	2.294	-1.570

<sup>a</sup>Comparison of the model-predicted elevation time series at the closest nodes to the Scituate Harbor tide gauge station for the CR grid without (CRNW) and with (CRWW) wave-current interaction and the HR grid without (HRNW) and with (HRWW) wave-current interaction. Time period: 00 GMT 23 December to 00 GMT 29 December.

closer to the coast before more rapid dissipation in the breaker/surf zone.

[25] The narrow harbor entrance zone formed by the two opposing breakwaters (called here the northern bandwidth (BW) and southern BW) and the long offshore breakwater (eastern BW) greatly reduced the wave energy flux into the harbor. This is shown in Figure 10 by the rapid drop in wave height along the transect T1–T2 (Figure 3) which starts at shore inside the harbor ( $x = 0$  m) and extends eastward through the entrance breakwater zone (centered near 650 m) out to 1500 m. Most of the decrease in wave height from  $\sim 4$  m at T2 to  $< 1$  m inside the harbor occurred within the entrance breakwater zone. Independent of grid resolution, the wave height at T2 was  $\sim 0.4$  m higher with wave-current interaction than without. As shown in Figure 10, the waves were heading WSW near T2 and then turned toward the west inside the narrow entrance. Inside the harbor, the waves spread toward the northern and southern shores inside the northern basin due to refraction and a lesser extent diffraction behind the breakwaters. Some waves continued to follow the main navigational channel as it turned southward into the southern basin. The CR- and HR-grid simulations produced similar wave patterns within the harbor, with additional small-scale variation seen in the HR grid simulation due to the improved resolution of the bathymetry.

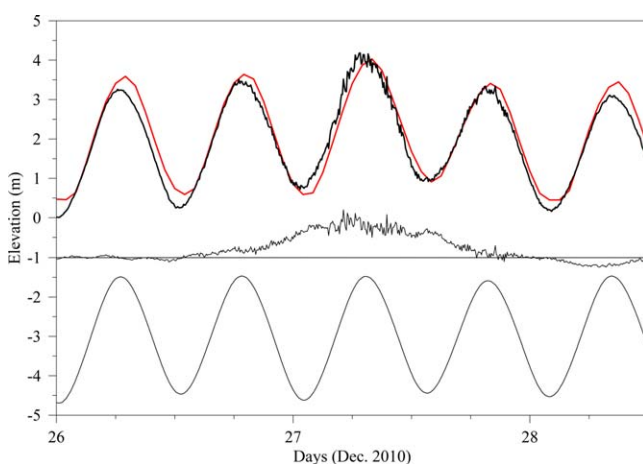


**Figure 11.** Top: tide gauge data (black) with HRWW model elevation +1.74 m (red). Middle: tide gauge data minus predicted tide offset by  $-1$  m. Bottom: predicted tide offset by  $-3$  m.

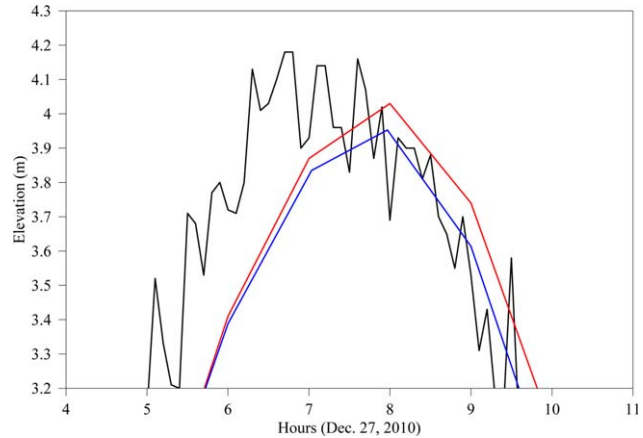


**Figure 12.** Tide gauge data (black), HRWW model elevation (red) and HRNW model elevation (blue) around the peak of the storm.

#### 4.2. Model Comparison With Scituate Harbor Tide Gauge Measurements

[26] We compare here time series of the water elevation measured at the Scituate Harbor tide gauge station with the water elevation predicted at the closest grid node for the two Scituate grids for the two cases, i.e., without and with wave-current interaction. This node was located 9.2 m (water depth 4.7 m) east of the tide gauge in the CR grid and 2.3 m (water depth 1.1 m) southeast of the tide gauge in the HR grid. The four model elevation time series were very similar, with maximum differences in mean (std) of 2.7 (1.3) cm (Table 4). The model elevation time series exhibited peak values at the same time (8 GMT 27 December) with little difference in the peak values ( $\leq 1$  cm) between CR and HR grid cases but an increase of 7.8 cm when wave-current interaction is included.

[27] Based on these model-model comparisons, we now focus on the HR grid model simulation with wave-current interaction and compare this time series with the harbor tide gauge time measurements, and, for reference, the tide only (computed using harmonic analysis on the tide gauge time series) (Figure 11). The model data is offset by the mean water elevation at the tide gauge ( $+1.74$  m) to account for the mean sea level in the western Mass Bay region off Scituate during December. The top plot (Figure 11) indicates that the model elevation is shifted below the tide gauge elevation prior to and after the storm but shows better agreement during the storm. The lower two plots show the decomposition of the tide gauge elevation into two components, the predicted tide and the “storm surge,” the difference between the tide gauge data and the predicted tide. The surge clearly starts on late 26 December and peaks early morning around 8 GMT 27 December before ending by early 28 December. The model underestimates the measured peak by  $\sim 15$  cm with a phase difference of  $\sim 45$  min (Figure 12). (For comparison, the HR model without wave-current interaction underestimates the measured peak by  $\sim 23$  cm with the same phase difference (Figure 12)). The storm-driven surge (maximum height  $\sim 0.9$  m) occurring during high tide (peak 1.52 m) explains the large extent of flooding during this nor’easter.

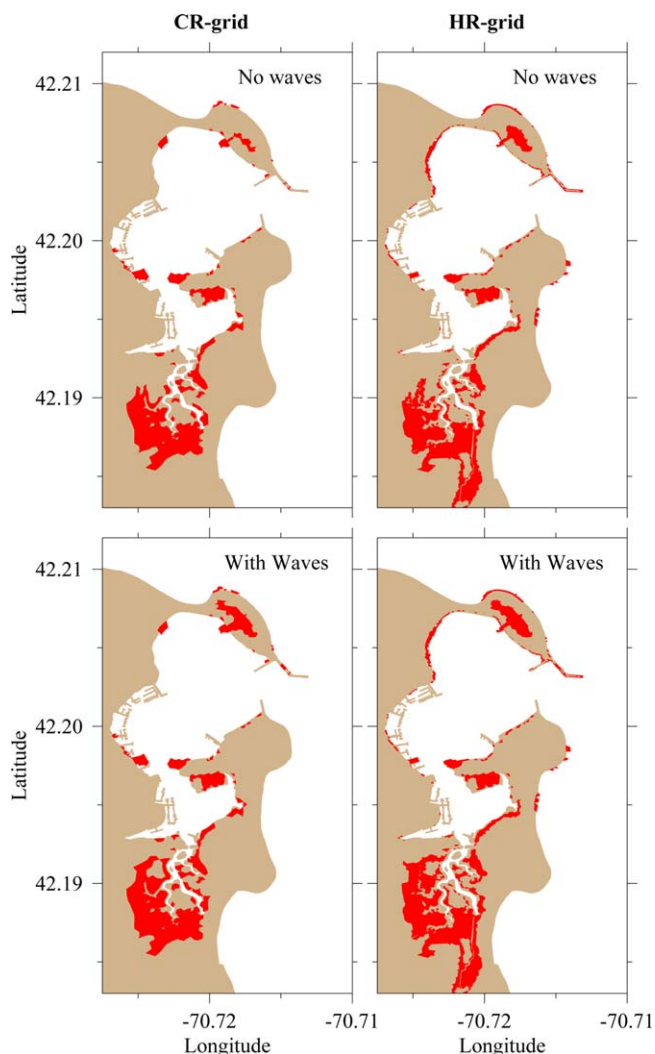


**Figure 13.** Map of the total land flooded during storm. Left panel: CR-grid; right panels: HR-grid. Top row: without wave-current interaction; bottom row: with wave-current interaction.

[28] Uncertainties in the model surface forcing could cause the peak surge underestimation and phase difference shown in Figure 11. Comparisons of the NECOFS/WRF-predicted surface wind and air pressure with NDBC 44013 measurements during the storm passage (Figure 7) show that (1) the buoy wind backed from NE to N before the model wind, and (2) the model underestimated the buoy air pressure drop by  $\sim 9$  hPa (36 hPa versus 45 hPa) and lagged the buoy by  $\sim 3.9$  h during 27 December. The SWAVE GOM3 simulation also underestimated the significant wave height by  $\sim 1.1$  m (7.2 m versus 6.1 m) and lagged the peak by  $\sim 1.8$  h during 27 December. The buoy peak wave period during this time was  $\sim 1$ – $2$  s longer than the model predicted. The surface wind stress was computed using the COARE2.6 wind drag coefficient. In comparison, the COARE4.0 drag coefficient increases more rapidly with wind speed above 12 m/s, becoming  $\sim 13\%$  larger at 20 m/s [Edson, 2009]. The potential underestimation of the surface wind stress and the underestimation and timing of the air pressure drop and wave field could all contribute to the

underestimation and lag in the model-simulated storm surge during 27 December shown in Figure 12.

[29] Comparisons of water elevation time series at the six reference sites inside the harbor also show that the HR-grid simulations with wave-current interaction produced the highest water elevations of the four cases. At site F on central Cedar Point, water had to rise over a low road (elevation  $\sim 2.1$  m) before flowing into a central depression surrounding site F. Without wave-current interaction, only the HR-grid simulation flooded site F. With wave-current interaction, both grids produced flooding, with the HR-grid slightly higher (15 cm). (See supporting information Appendix A for the six site locations and the model-model elevation comparisons.)

### 4.3. Inundation

[30] The model-data and model-model comparisons of water elevation presented above imply that the HR-grid with wave-current interaction simulation would produce the maximum inundation. This is seen in maps of the total land flooded during the storm passage (Figure 13). In particular, with the higher spatial resolution on Cedar Point and in the large marsh area south of the Edward Foster Road causeway (Figure 3, transect c1–c2), more area has been flooded. The storm surge started to build during the flood tide on the afternoon of 26 December, and continued to build on the following flood tide to its maximum around 08 GMT 27 December, a result of a reduced outflow from the harbor during the intervening ebb tide and increased inflow into the harbor on the 27 December flood tide. The surge disappeared during the enhanced ebb and reduced flood tide cycle. (See supporting information Appendix B for time series of transport through the harbor entrance and the other two transects shown in Figure 3.)

### 4.4. Currents

[31] Why does the inclusion of wave-current interaction independent of grid resolution increase the inundation within Scituate Harbor during this storm? Maps of the HR-grid model-simulated depth-averaged currents with wave-current interaction during the peak of the storm (Figure 14) show the formation of a stagnation point on the northeast side of Cedar Point (located near  $42.207^\circ\text{N}$ ,  $-70.716^\circ\text{E}$  during the peak of the storm). (See supporting information Appendix C for the corresponding CR-grid model current maps.) North of this stagnation point, the nearshore currents flow northwest of this point instead of southeast in the cases without wave-current interaction. South of this stagnation point, the nearshore currents rapidly accelerate to greater speeds around the harbor entrance zone and along the two southern headlands. The formation of this stagnation point is a direct result of the local concentration of the wave-induced radiation stress and convergence in both alongshore directions due to the northwest-southeast orientation of Cedar Point and the offshore extent of its nearshore bathymetry. The large increase in alongshore currents south of this stagnation point is due to the concentration of radiation stress and convergence along the eastern face of First Cliff and Second Cliff (See supporting information Appendix D for maps of the depth-averaged wave radiation stress during the storm.)

[32] A separate stagnation point forms on the northeast corner of First Cliff ( $42.1998^\circ\text{N}$ ,  $-70.7145^\circ\text{E}$ ) in all cases

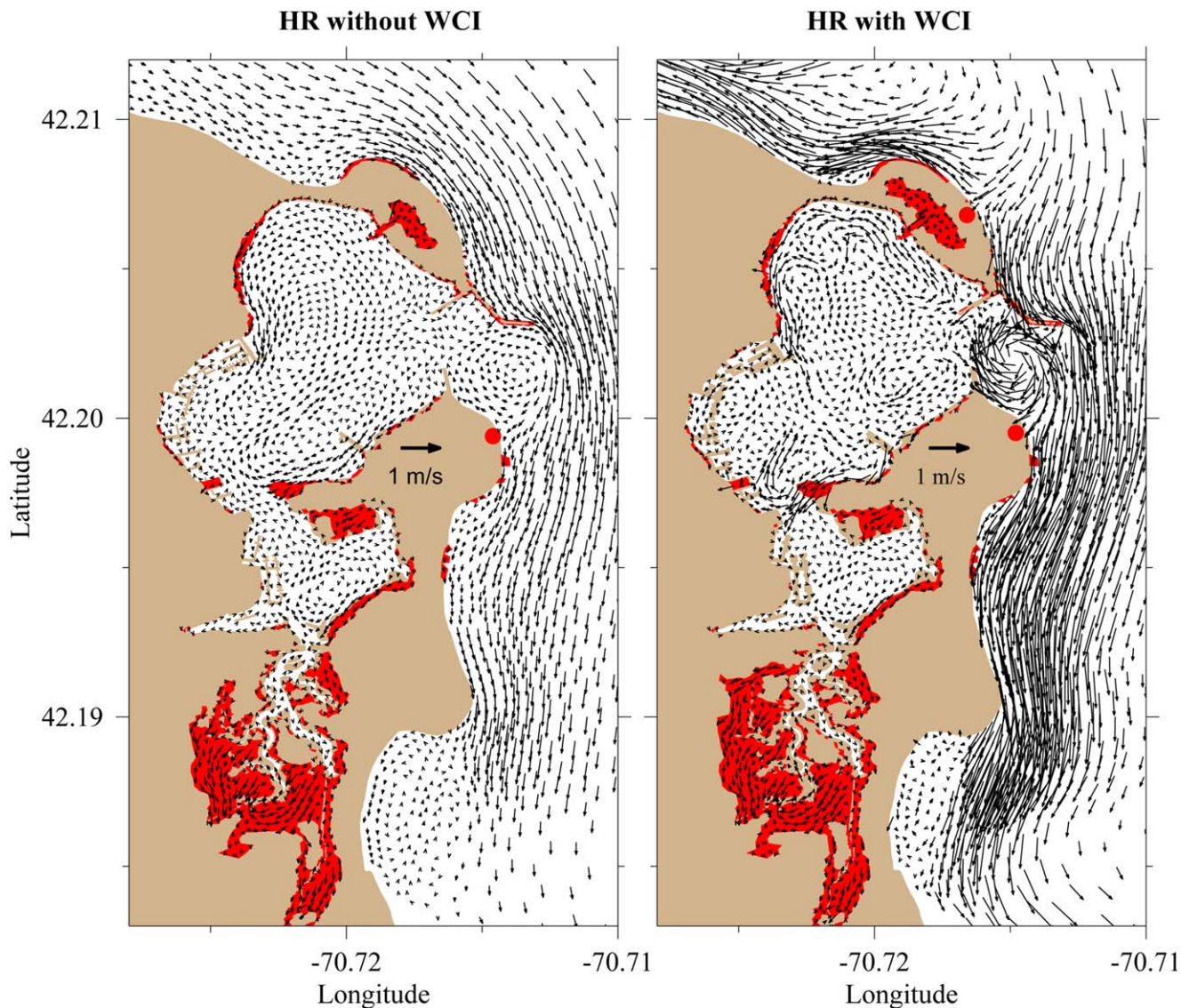


**Figure 14.** Maps of depth-averaged current at 08 GMT 27 December simulated with the HR grid without wave current interaction (left) and with wave-current interaction (right). Flooded areas denoted by red. The stagnation point on Cedar Point is indicated by a red circle in the right map while the stagnation point on First Cliff is indicated by a red circle in both maps. (See Appendix C for corresponding maps simulated with the CR grid.)

during the storm passage (Figure 15). Located where the coastline and nearshore isobaths change direction by  $\sim 45^\circ$ , pointing northwestward into the harbor entrance zone and south along the headland, this stagnation point separates southwestward onshore flow into one stream turning into the harbor entrance zone and another stream heading generally southward down the coast. The location of this stagnation point appears to be locked to the local bathymetry, and local flow separation can be seen during both the flood tide (when much of the inflow into the harbor comes from the north around the eastern BW) and ebb tide (when the harbor outflow through the entrance creates a clockwise separation eddy along the southern BW).

[33] A clockwise separation eddy is generated by the eastern BW in all cases during the storm passage (Figure 15). However, with wave-current interaction, the depth-

averaged currents within this eddy are significantly stronger (Figure 14). On 26 December the morning before the storm's arrival, a weak separation eddy forms along the southern side of the eastern BW during the flood tide and a weak clockwise separation eddy forms east of the southern BW during the ebb tide as part of the normal tidal cycle during calm weather. As the storm intensity starts to build during 26 December afternoon and night, the eastern BW separation eddy grows in size and strength. Maps of depth-averaged current for 27 December (Figure 15) show the increase in the nearshore flow toward the eastern BW tip to  $\sim 1.0$ – $1.2$  m/s and temporal change in the eddy shape and strength. As the eddy strengthens in the period before high tide ( $\sim 7:20$  GMT), more flow is directed through the entrance into the harbor. During the following ebb tide, the harbor outflow through the entrance joins the separation

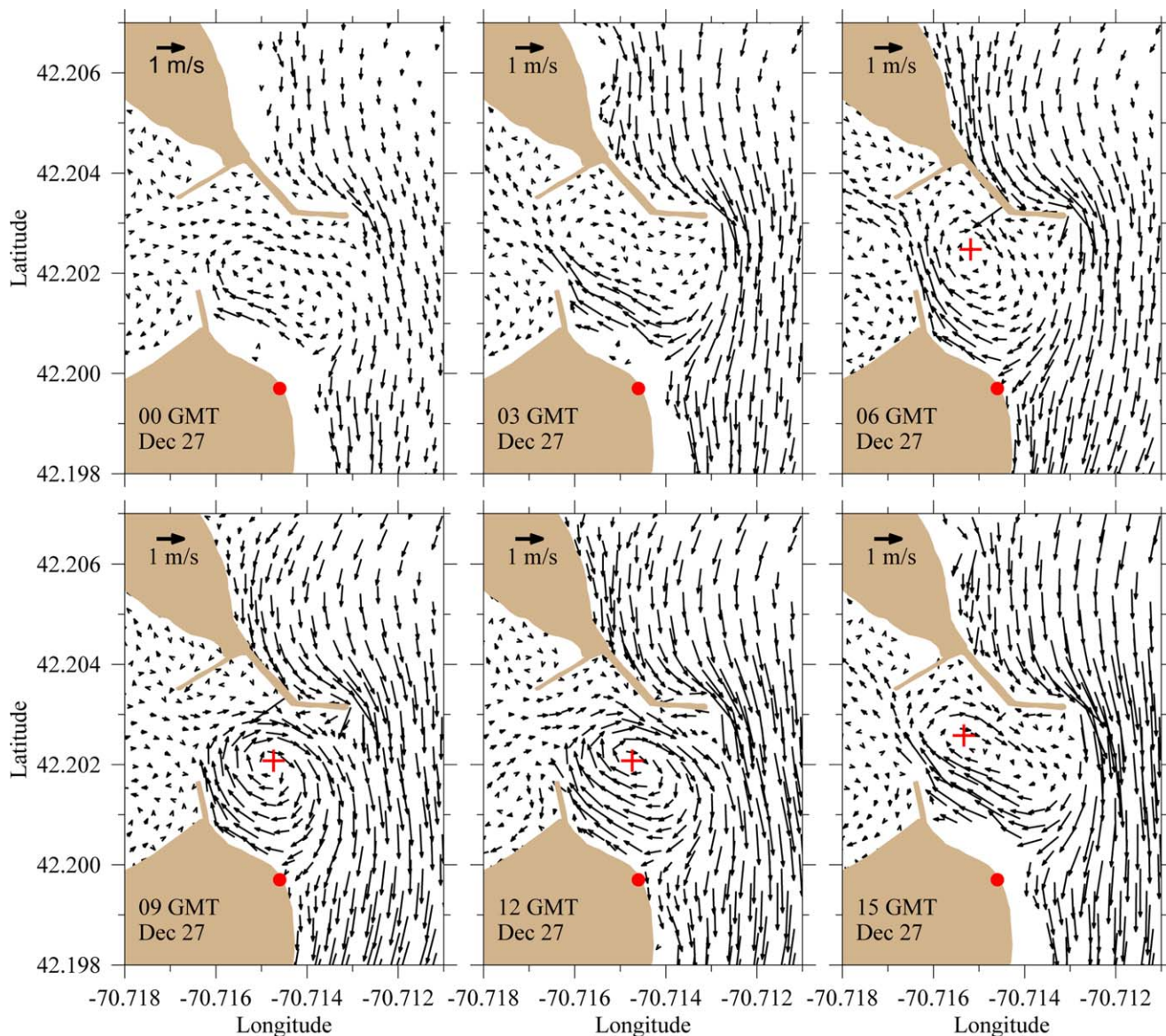


**Figure 15.** Sequence of maps of depth-averaged current in and near the harbor entrance for the HR-grid case with wave-current interaction at 00, 03, 06, 09, 12 and 15 GMT 27 December. The model-simulated first high tide on 27 December occurred at 7:20 GMT. The stagnation point on First Cliff is indicated by a red circle in each map and the approximate center of the clockwise eddy in the entrance zone is shown by a red cross.

eddy eastward flow, shifting the eddy center to the south and becoming weaker at low tide. The eddy exhibits similar temporal behavior during the next flood-ebb cycle, in part because of the relative slow decay of the onshore wave field. The southward nearshore flow along First Cliff reaches speeds of  $\sim 1.0\text{--}1.4$  m/s during the peak storm surge (Figure 14).

[34] The structure of the eastern BW separation eddy is also seen in plots of the depth-averaged currents along the T1–T2 transect near peak surge in Figure 16. Near T2, the currents are oriented roughly southwest, increase in magnitude, and rotate counterclockwise toward south near the tip of the eastern BW ( $x = 885$  m), reaching a maximum of  $\sim 1.1$  m/s oriented almost due south about  $\sim 70$  m east of the BW tip. This increase is due both to the eastward extension

of the eddy and to the increase in alongshore wave-driven current as the waves shoal over the inner shelf. Within the separation eddy ( $x \sim 600$  to  $930$  m), the southward current rapidly decreases and becomes northward while the eastward current reaches a maximum of  $\sim 0.6$  m/s around  $x \sim 800$  m. This wind and wave-driven eddy has a mean vertical vorticity of roughly  $5 \times 10^{-3} \text{ s}^{-1}$ . This highly nonlinear breakwater separation eddy and wave-current interaction combine to produce a setup of  $\sim 8$  cm within the entrance, independent of grid resolution within the harbor.

## 5. Conclusions

[35] A nested FVCOM inundation forecast model system for Scituate has been developed as part of the Northeast

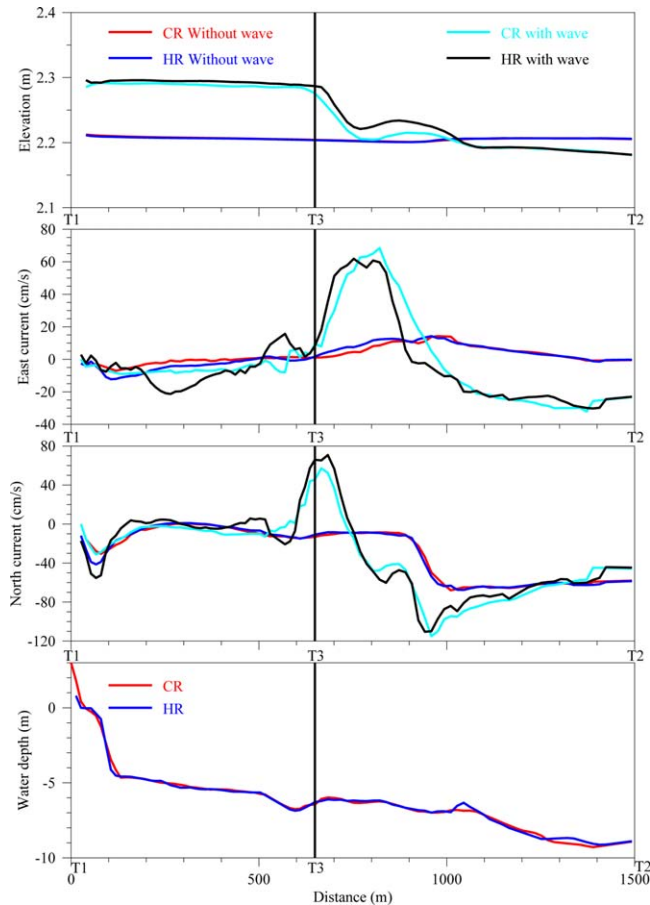


**Figure 16.** Surface elevation (m), east and north current components ( $\text{cm s}^{-1}$ ), and bottom depth along the T1-T2 transect. The entrance center (T3) is located at  $x = 650$  m from shore. (See Figure 3 for transect location.)

Coastal Ocean Forecast System (NECOFS). Scituate Harbor contains two shallow basins aligned roughly north-south and is formed by northern and southern promontories with seawalls built along their eastern sides. The harbor is entered through a set of three breakwaters with a roughly 60 m wide by 6 m deep navigation channel. NECOFS was used here to hindcast coastal flooding in Scituate during the 27 December 2010 nor'easter. This extratropical cyclone strengthened into a gale as it approached Cape Cod on late 26 December and produced peak winds of  $\sim 22$  m/s and  $\sim 7.5$  m waves from the northeast off Scituate during early 27 December during flood tide. The combination of the storm-driven surge peaking near  $\sim 0.9$  m within 1 h of high tide at  $\sim 1.5$  m plus seasonal higher mean water level produced significant inundation in Scituate.

[36] The Scituate FVCOM inundation model included flooding/drying, seawall/breakwater, and wave-current interaction capabilities, and was driven by one-way nesting with NECOFS. Four hindcasts were made using both coarse-resolution (CR) and high-resolution (HR) grids with and without inclusion of wave-current interaction. Without wave-current interaction, the wind-driven nearshore depth-averaged currents flowed southward, with an attached separation eddy forming downstream of the eastern breakwater. With wave-current interaction, a stagnation point formed

on the northern promontory, causing the nearshore currents to flow northwestward. South of this stagnation point, the nearshore currents accelerated to greater speeds around the harbor entrance and southern promontory, with significantly increased currents greater than 1 m/s in the entrance separation eddy. This eddy was highly nonlinear with large lateral shear rates of order  $5 \times 10^{-3} \text{ s}^{-1}$ . In all cases, the waves incoming through the entrance breakwaters were reduced to  $\leq 1$  m height inside the harbor. Comparisons of the model-simulated water elevation time series with the harbor tide gauge station measurements showed that wave-current interaction increased the peak model surge by  $\sim 8$  cm independent of grid resolution in closer agreement with the observed peak. Increased resolution within the harbor produced greater flooding in several shallow areas but did not significantly change the maximum water level in the main harbor.

[37] This hindcast study of inundation within Scituate Harbor during the 27 December 2010 nor'easter has highlighted the importance of wave-current interaction. In particular, the radiation stress generated by the large wind-driven shoaling waves over the inner shelf created the stagnation point on the northern promontory, changing the direction and strength of the depth-averaged alongshore currents, greatly enhancing the separation eddy created by the eastern breakwater and increasing the surge into the harbor.

[38] This suggests that including wave-current interaction in both the NECOFS regional and nested Scituate inundation forecasts will improve the accuracy of the local inundation forecast. (The need to include wave-current interaction in regional 3-D simulations of tropical storm inundation has also been demonstrated by *Sheng et al.* [2010], *Sun et al.* [2013], and others). The present computational efforts required to run FVCOM and SWAVE coupled using the same time step for the regional and Scituate simulations are large. However, we plan to use the Earth System Modeling Framework (ESMF) to enable the coupled FVCOM-SWAVE system to run with longer time steps for SWAVE, thus significantly reducing the computational effort. In addition, we plan to use our improved understanding of the processes controlling inundation in Scituate Harbor to develop a new grid optimized for operational forecasting.

[39] We have used NECOFS and the present Scituate FVCOM inundation model and SWAVE with wave-current interaction to hindcast inundation during the 27 December 2012 nor'easter (Winter Storm Euclid) and forecast inundation during the 7 and 8 February 2013 nor'easter (Winter Storm Nemo) with useful results based on feedback from Taunton WFO (R. Thompson, personal communication, 2013) and Scituate (N. Duggan, personal communication, 2013). Based on our experience with Scituate Harbor inundation, we are presently setting up local FVCOM inundation forecast model systems for the Hampton-Seabrook estuary, NH and other sites to be driven through nesting with NECOFS.

[40] In addition to the flooding that occurred within Scituate Harbor during the 27 December 2010 nor'easter, wave overtopping caused significant flooding and property damage along the coast north of Scituate Harbor. Wave overtopping of seawalls has two primary forms: (1) when

waves run up the face and over the seawall, producing “green water” discharge over the top of the seawall, and (2) when waves break as they approach the seawall and send plumes of water high enough to be carried over the seawall (also called “splash-over”). Wave overtopping occurs around the world and estimating the water volume transport over the seawall top is the focus of ongoing research by many groups (e.g., U.S. Army Corps of Engineers [CEM, 2002], Pullen et al. [2007]; Allsop et al. [2005]). Both forms of wave overtopping are common during strong storms in the Northeast but this process is not included in NECOFS or other regional inundation models (to our understanding). We plan to develop with others a FVCOM wave overtopping module that can be used for Scituate and other NECOFS inundation forecast sites.

[41] **Acknowledgments.** This project was supported by NOAA via the U.S. IOOS Office (Award: NA10NOS0120063 and NA11NOS0120141) and was managed by the Southeastern Universities Research Association. The Scituate FVCOM setup was supported by the NOAA-funded IOOS NERACOOS program for NECOFS and the MIT Sea grant College Program through grant 2012-R/RC-127. C. Chen serves as chief scientist for the International Center for Marine Studies, Shanghai Ocean University, and his contribution was supported by the Program of Science and Technology Commission of Shanghai Municipality (09320503700). We want to thank R. Signell (USGS) for his generous and continuing advice with obtaining and using the latest bathymetry and LiDAR data in the development of the NECOFS regional and Scituate FVCOM inundation forecast model grids. This model validation aspect of this project was not possible without the in situ tide station data collected in Scituate Harbor prior and during the 27 December 2010 nor’easter. R. Thompson (NWS Taunton (MA) WFO) coordinated funding for this tide station through NOAA’s North Atlantic Regional Team. This tide station was designed and installed by the Charybdis Group team of F. Peri and M. Pollard, who also provided this project with the final edited data. Conversations with J. Burtner (Mass CZM), Scituate town officials M. Patterson and N. Duggan, and Cedar Point resident D. Ball were very helpful. We also want to acknowledge the continuing encouragement and support for coastal inundation modeling and forecasting by J. Trowbridge (WHOI), R. Morrison (NERACOOS), J. Cannon (NWS Grey (ME) WFO), A. Mignone (NWS Caribou (ME) WFO), R. Luettich (UNC), J. Westerlink (UND), and other members of the extratropical inundation modeling group and N. Dill (Woods Hole Group), who provided useful information about wave overtopping. This manuscript has been significantly improved by input from two reviewers.

## References

- Allsop, W., T. Bruce, J. Pearson, and P. Besley (2005), Wave overtopping at vertical and steep seawalls, *Proc. ICE Mar. Eng.*, *158*(MA3), 103–114.
- CEM (2002), Coastal Engineering Manual (EM 1110-2-1100), Part VI, chap. 5. Coastal and Hydraulics Laboratory, Engineer Research and Development Center, Waterways Experiment Station, Vicksburg, Mississippi. [Available at [http://140.194.76.129/publications/eng-manuals/EM\\_1110-2-1100\\_vol/PartVI/cem-vi-5.pdf](http://140.194.76.129/publications/eng-manuals/EM_1110-2-1100_vol/PartVI/cem-vi-5.pdf).]
- Chen, C., R. C. Beardsley, and P. J. S. Franks (2001), A 3-D prognostic model study of the ecosystem over Georges Bank and adjacent coastal regions. Part I: Physical model, *Deep Sea Res., Part II*, *48*, 419–456.
- Chen, C., H. Liu, and R. Beardsley (2003), An unstructured grid, finite-volume, three dimensional, primitive equations ocean model: Application to coastal ocean and estuaries, *J. Atmos. Oceanic Technol.*, *20*(1), 159–186.
- Chen, C., R. C. Beardsley, S. Hu, Q. Xu, and H. Lin (2005), Using MM5 to hindcast the ocean surface forcing fields over the Gulf of Maine and Georges Bank region, *J. Atmos. Oceanic Technol.*, *22*(2), 131–145.
- Chen, C., R. C. Beardsley, and G. Cowles (2006a), An unstructured grid, finite-volume coastal ocean model (FVCOM) system, Special Issue entitled “Advances in Computational Oceanography”, *Oceanography*, *19*(1), 78–89.
- Chen, C., G. Cowles, and R. C. Beardsley (2006b), An unstructured-grid, finite-volume coastal ocean model: FVCOM user manual, 2nd ed. *Tech. Rep. SMAS/UMASSD-06-0602*, 315 pp.
- Chen, C., H. Huang, R. C. Beardsley, Q. Xu, R. Limeburner, G. W. Cowles, Y. Sun, J. Qi, and H. Lin (2011), Tidal dynamics in the Gulf of Maine and New England Shelf: An application of FVCOM, *J. Geophys. Res.*, *116*, C12010, doi:10.1029/2011JC007054.
- Chen, C., et al. (2013), Extratropical storm inundation testbed: Inter-model comparisons in Scituate, Massachusetts, *J. Geophys. Res.*, *118*, 1–20, doi:10.1002/JGRC.20397.
- Donelan, M. A., F. W. Dobson, S. D. Smith, and R. J. Anderson (1993), On the dependence of sea surface roughness on wave development, *J. Phys. Oceanogr.*, *23*(9), 2143–2149.
- Edson, J. (2009), Review of air-sea transfer processes, paper presented at ECMWF Workshop 2008 on Ocean-Atmosphere Interactions, Reading, England.
- Egbert, G. D., and S. Y. Erofeeva (2002), Efficient inverse modeling of barotropic ocean tides, *J. Atmos. Oceanic Technol.*, *19*(2), 183–204, doi:10.1175/1520-0426(2002)019<0183:EIMOBO>2.0.CO;2.
- Fairall, C. W., E. F. Bradley, D. P. Rogers, J. B. Edson, and G. S. Young (1996), Bulk parameterization of air-sea fluxes for TOGA COARE, *J. Geophys. Res.*, *101*(C2), 3747–3764.
- Foreman, M., R. Walters, R. Henry, C. Keller, and A. Dolling (1995), A tidal model for eastern Juan de Fuca Strait and the southern Strait of Georgia, *J. Geophys. Res.*, *100*(C1), 721–740.
- García-Lafuente, J., J. Delgado, G. Navarro, C. Calero, M. Díez-Minguito, J. Ruiz, and J. Sánchez-Garrido (2012), About the tidal oscillations of temperature in a tidally driven estuary: The case of Guadalquivir estuary, southwest Spain, *Estuarine Coastal Shelf Sci.*, *111*, 60–66.
- Ge, J., C. Chen, J. Qi, P. Ding, and R. C. Beardsley (2012), A dike-groynes algorithm in a terrain-following coordinate ocean model (FVCOM): Development, validation and application, *Ocean Modell.*, *47*, 26–40, doi:10.1016/j.ocemod.2012.01.006.
- Hong, S.-Y., and H.-L. Pan (1996), Nonlocal boundary layer vertical diffusion in a medium-range forecast model, *Mon. Weather Rev.*, *124*, 2322–2339.
- Hubbard, M. E. (1999), Multidimensional slope limiters for MUSCLtype finite volume schemes on unstructured grids, *J. Comput. Phys.*, *155*, 54–74.
- Hu, S. (2009), Variability of physical forcing and their impacts on nutrient supplies and fall phytoplankton blooms in the Gulf of Maine-Georges Bank region, Ph.D. thesis, pp. 237, University of Massachusetts Dartmouth, School of Marine Science and Technology, New Bedford, Massachusetts.
- Kobayashi, M. H., J. M. C. Pereira, and J. C. F. Pereira (1999), A conservative finite-volume second-order-accurate projection method on hybrid unstructured grids, *J. Comput. Phys.*, *150*, 40–75, doi:10.1006/jcph.1998.6163.
- Loder, J. W., C. G. Hannah, B. D. Petrie, and E. A. Gonzalez (2003), Hydrographic and transport variability on the Halifax section, *J. Geophys. Res.*, *108*(C11), 8003, doi:10.1029/2001JC001267.
- Mellor, G. L., and T. Yamada (1982), Development of a turbulence closure model for geophysical fluid problem, *Rev. Geophys.*, *20*(4), 851–875.
- Pawlowicz, R., B. Beardsley, and S. Lentz (2002), Classical tidal harmonic analysis with error analysis in MATLAB using T\_TIDE, *Comput. Geosci.*, *28*, 929–937.
- Pringle, J. (2006), Sources of variability in Gulf of Maine circulation, and the observations needed to model it, *Deep Sea Res., Part II*, *53*, 2457–2476.
- Pullen, T., W. H. Allsop, T. Bruce, A. Kortenhuis, H. Schüttrumpf, and J. W. van der Meer (2007), *Eurotop Wave Overtopping of Sea Defences and Related Structures: Assessment Manual*, ISSN 0452-7739, ISBN 978-3-8042-1064-6. [Available at <http://www.overtopping-manual.com/eurotop.pdf>.]
- Qi, J., C. Chen, R. C. Beardsley, W. Perrie, Z. Lai, and G. Cowles (2009), An unstructured-grid finite-volume surface wave model (FVCOM-SWAVE): Implementation, validations and applications, *Ocean Modell.*, *28*, 153–166, doi:10.1016/j.ocemod.2009.01.007.
- Roworth, E., and R. P. Signell (1998), Construction of digital bathymetry for the Gulf of Maine, *Open File Rep. 98-801*, Coastal and Mar. Geol. Prog. U.S. Geol. Surv., Woods Hole, Mass.
- Schwing, F. B. (1989), Subtidal response of the Scotian Shelf bottom pressure field to meteorological forcing, *J. Atmos. Oceanic Technol.*, *27*, 157–180.
- Sheng, Y. P., V. Alymov, and V. A. Paramygin (2010), Simulation of storm surge, wave, currents, and inundation in the Outer Banks and Chesapeake Bay during Hurricane Isabel in 2003: The importance of waves, *J. Geophys. Res.*, *115*, C04008, doi:10.1029/2009JC005402.

- Smagorinsky, J. (1963), General circulation experiments with the primitive equations. I. The basic experiment, *Mon. Weather Rev.*, *91*, 99–164.
- Smith, P. C., and F. B. Schwing (1991), Mean circulation and variability on the eastern Canadian continental shelf, *Cont. Shelf Res.*, *11*(8–10), 977–1012.
- Sun, Y., C. Chen, R. Beardsley, Q. Xu, J. Qi, and H. Lin (2013), Impact of current-wave interaction on storm surge simulation: A case study for Hurricane Bob, *J. Geophys. Res.*, *118*, 2685–2701, doi:10.1002/JGRC.20207.
- Warner, J. C., S. R. Christopher, R. P. Signell, C. Harris, and H. G. Arango (2008), Development of a three-dimensional, regional, coupled wave, current, and sediment-transport model, *Comput. Geosci.*, *34*, 1284–1306, doi:10.1016/j.cageo.2008.02.012.
- Werner, S. R., R. C. Beardsley, S. J. Lentz, D. L. Hebert, and N. S. Oakey (2003), Observations and modeling of the tidal bottom boundary layer on the southern flank of Georges Bank, *J. Geophys. Res.*, *108*(C11), 8005, doi:10.1029/2001JC001271.
- Wu, L., C. Chen, F. Guo, M. Shi, J. Qi, and J. Ge (2010), A FVCOM-based unstructured grid wave, current, sediment transport model, I. Model description and validation, *J. Ocean Univ. China*, *10*(1), 1–8, doi: 10.1007/s11802-011-1788-3.